

Steady-State Entanglement Generation via Casimir-Polder Interactions

Mohsen Izadyari,^{1,2,*} Onur Pusuluk,^{2,†} Kanu Sinha,^{3,‡} and Özgür E. Müstecaplıoğlu^{1,4,5,§}

¹*Department of Physics, Koç University, 34450 Sarıyer, Istanbul, Türkiye*

²*Faculty of Engineering and Natural Sciences, Kadir Has University, 34083 Fatih, Istanbul, Türkiye*

³*College of Optical Sciences and Department of Physics, University of Arizona, Tucson, AZ, 85721, USA*

⁴*TÜBİTAK Research Institute for Fundamental Sciences, 41470 Gebze, Türkiye*

⁵*Faculty of Engineering and Natural Sciences, Sabanci University, 34956 Tuzla, Istanbul, Türkiye*

We investigate the generation of steady-state entanglement between two atoms resulting from the fluctuation-mediated Casimir-Polder (CP) interactions near a surface. Starting with an initially separable state of the atoms, we analyze the atom-atom entanglement dynamics for atoms placed at distances in the range of ~ 25 nm away from a planar medium, examining the effect of medium properties and geometrical configuration of the atomic dipoles. We show that perfectly conducting and superconducting surfaces yield an optimal steady-state concurrence value of approximately 0.5. Furthermore, although the generated entanglement decreases with medium losses for a metal surface, we identify an optimal distance from the metal surface that assists in entanglement generation by the surface. While fluctuation-mediated interactions are typically considered detrimental to the coherence of quantum systems at nanoscales, our results demonstrate a mechanism for leveraging such interactions for entanglement generation.

Introduction—Nanoscale quantum systems enable efficient and tunable light-matter interactions by confining EM fields in small mode volumes [1–6]. Such systems hold enormous promise in the development of photonic devices that exhibit nonlinearities at the single-photon level [7–10], building efficient light-matter interfaces [11–16] that are essential for various quantum information processing tasks [17, 18], as well as, exploring fundamental phenomena such as ultrafast dynamics at the nanoscale [19, 20].

However, as quantum systems move towards nanoscales, while the coupling between atomic systems and the relevant modes of the EM field increases, so does the detrimental interaction of atomic systems with the quantum fluctuations of the EM field [21]. For example, fluctuation-induced Casimir-Polder (CP) interactions [22, 23] between neutral polarizable particles and nearby surfaces [24–26] critically limit trapping schemes and the coherence of quantum emitters near surfaces [27, 28].

The realization of practical quantum technologies requires the production and longevity of quantum coherence and entanglement [29, 30]. To this end, sophisticated quantum control methods and environmental noise engineering or noise-assisted entanglement generation schemes have been proposed [31–37]. Given that fluctuation-mediated interactions are deleterious for quantum coherence and correlations of atomic systems near surfaces [38–49], engineering such fluctuation phenomena to achieve better coherence and control of nanoscale quantum systems thus becomes a vital goal in developing nanoscale quantum devices [18]. Furthermore, the possibility of appropriately manipulating these fluctuation-mediated interactions and turning them into a useful tool can be thus doubly advantageous [50].

In this Letter, we propose a simple and intuitive scheme for controlling fluctuation phenomena to produce steady-state entanglement between two quantum emitters near a surface. Our approach utilizes the effective coherent coupling between the atoms in the presence of a medium that dominates their surface-modified decoherence to produce robust quantum entanglement in the steady state for critical placement of the atoms relative to the surface.

Model—We present a system of two emitters positioned at a distance x from each other and at a distance z from a planar half-space medium characterized by electric permittivity $\epsilon(\omega)$ (Fig. 1). Each emitter, denoted by $i = 1, 2$ for the first and second emitter respectively, is modeled as a two-level system with ground state $|g\rangle_i$ and excited state $|e\rangle_i$, with a resonant transition frequency ω_0 . In the presence of the planar surface, the electric

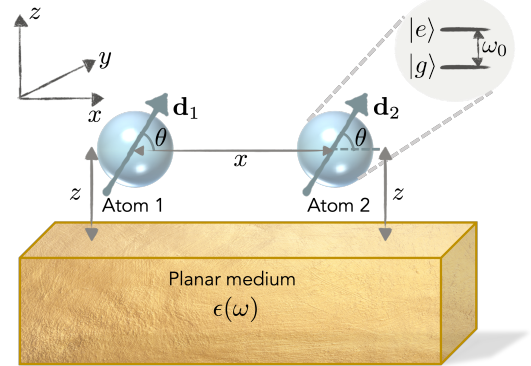


FIG. 1. Schematic of the model featuring two two-level atoms near a planar medium of permittivity $\epsilon(\omega)$. The atomic dipoles \mathbf{d}_1 and \mathbf{d}_2 are oriented along θ with respect to the x -axis.

field originating from vacuum fluctuations at position \mathbf{r} is defined as [51]:

$$\hat{E}(\mathbf{r}) = \sum_{\lambda=e,m} \int d^3\mathbf{r}' \int d\omega [\bar{G}_\lambda(\mathbf{r}, \mathbf{r}', \omega) \cdot \hat{f}_\lambda(\mathbf{r}', \omega) + \text{H.c.}] \quad (1)$$

Here, $\hat{f}_\lambda(\mathbf{r}, \omega)$ and $\hat{f}_\lambda^\dagger(\mathbf{r}, \omega)$ are bosonic annihilation and creation operators, representing noise polarization ($\lambda = e$) and magnetization ($\lambda = m$) excitations at frequency ω . The coefficients $\bar{G}_\lambda(\mathbf{r}, \mathbf{r}', \omega)$ are related to the Green's tensor $\bar{G}(\mathbf{r}, \mathbf{r}', \omega)$, which satisfies the inhomogeneous Helmholtz equation in the presence of the medium (See SM for details). The propagator $\bar{G}(\mathbf{r}, \mathbf{r}', \omega) = \bar{G}_{\text{free}}(\mathbf{r}, \mathbf{r}', \omega) + \bar{G}_{\text{sc}}(\mathbf{r}, \mathbf{r}', \omega)$ consists of the free space and scattering components. The total Hamiltonian, denoted as $\hat{H}_T = \hat{H}_S + \hat{H}_F + \hat{H}_{\text{int}}$, comprises of the atomic Hamiltonian $\hat{H}_S = \sum_{i=1}^2 \hbar\omega_0 \hat{\sigma}_i^+ \hat{\sigma}_i^-$, the surface-assisted electromagnetic field in vacuum state \hat{H}_F , and the interaction Hamiltonian. $\hat{\sigma}_i^\pm = (\hat{\sigma}_i^\mp)^\dagger = |e\rangle_i \langle g|_i$ indicate the ladder operators for the atomic transition. The interaction Hamiltonian is described by $\hat{H}_{\text{int}} = -\sum_{i=1}^2 \hat{d}_i \cdot \hat{E}(\mathbf{r}_i)$, where $\hat{d}_i = \mathbf{d}_i \hat{\sigma}_i^+ + \mathbf{d}_i^* \hat{\sigma}_i^-$ represents the electric-dipole operator associated with the i -th emitter located at position \mathbf{r}_i , with \mathbf{d}_i denoting the electric dipole moment.

The time evolution of the density matrix ρ_S for the emitters is governed by the Born-Markov master equation [52]:

$$\frac{d\hat{\rho}_S}{dt} = -\frac{i}{\hbar} [\hat{\mathcal{H}}_{\text{eff}}, \hat{\rho}_S] + \mathcal{L}_{\text{eff}}[\hat{\rho}_S] \quad (2)$$

Here $\hat{\mathcal{H}}_{\text{eff}}$ is the atomic effective Hamiltonian in interaction picture defined by [26, 53, 54]

$$\hat{\mathcal{H}}_{\text{eff}} = \hbar \left[\sum_{i=1,2} \left(\Omega_i^{(+)}(\mathbf{r}_i) \hat{\sigma}_i^+ \hat{\sigma}_i^- + \Omega_i^{(-)}(\mathbf{r}_i) \hat{\sigma}_i^- \hat{\sigma}_i^+ \right) + \sum_{i \neq j} \Omega_{ij}(\mathbf{r}_i, \mathbf{r}_j) \hat{\sigma}_i^- \hat{\sigma}_j^+ \right], \quad (3)$$

and the effective surface-modified Liouvillian in Eq. (2) is given by

$$\begin{aligned} \mathcal{L}_{\text{eff}}[\hat{\rho}_S] &= \sum_{ij} \frac{\Gamma_{ij}(\mathbf{r}_i, \mathbf{r}_j)}{2} (2\hat{\sigma}_i^- \hat{\rho}_S \hat{\sigma}_j^+ - \hat{\sigma}_i^+ \hat{\sigma}_j^- \hat{\rho}_S - \hat{\rho}_S \hat{\sigma}_i^+ \hat{\sigma}_j^-), \end{aligned} \quad (4)$$

where $\Gamma_{ij}(\mathbf{r}_i, \mathbf{r}_j) = \Gamma_{ij}^{\text{free}}(\mathbf{r}_i, \mathbf{r}_j) + \Gamma_{ij}^{\text{sc}}(\mathbf{r}_i, \mathbf{r}_j)$ corresponds to the dissipative coupling coefficient between two atoms, while Γ_{ii} represents the spontaneous emission rate for the excited state of the i th atom.

The diagonal elements of the effective Hamiltonian $\hat{\mathcal{H}}_{\text{eff}}$ are the CP shift contributions defined as:

$$\begin{aligned} \Omega_i^{(-)}(\mathbf{r}_i) &= \frac{\mu_0 \omega_0}{\pi} \int_0^\infty \frac{d\zeta \zeta^2}{\zeta^2 + \omega^2} \mathbf{d}_i^* \cdot [\bar{G}_{\text{sc}}(\mathbf{r}_i, \mathbf{r}_i, i\zeta)] \cdot \mathbf{d}_i \\ \Omega_i^{(+)}(\mathbf{r}_i) &= -\Omega_i^{(-)}(\mathbf{r}_i) + \Omega_i^{\text{res}}(\mathbf{r}_i), \end{aligned} \quad (5)$$

where, the free component of Green's tensor is neglected, assuming it has already been taken into account as a contribution to Lamb shifts in the bare levels. Additionally, the resonant contribution $\Omega_i^{\text{res}}(\mathbf{r}_i) = -\mu_0 \omega_0^2 \text{Re}[\mathbf{d}_i^* \cdot \bar{G}_{\text{sc}}(\mathbf{r}_i, \mathbf{r}_i, \omega_0) \cdot \mathbf{d}_i]$, is dependent exclusively on the environment's response at the resonant frequency where μ_0 is the Permeability of free space.

The off-diagonal elements ($i \neq j$) of the effective Hamiltonian, along with the dissipative coupling coefficients, are determined by the resonant contribution of the real and imaginary parts of Green's function. This is expressed as $\Omega_{ij}(\mathbf{r}_i, \mathbf{r}_j) = \Omega_{ij}^{\text{free}}(\mathbf{r}_i, \mathbf{r}_j) + \Omega_{ij}^{\text{sc}}(\mathbf{r}_i, \mathbf{r}_j)$ as follows:

$$\begin{aligned} \Omega_{ij}^{\text{free,sc}}(\mathbf{r}_i, \mathbf{r}_j) &= -\mu_0 \omega_0^2 \text{Re}[\mathbf{d}_i^* \cdot \bar{G}_{\text{free,sc}}(\mathbf{r}_i, \mathbf{r}_j, \omega_0) \cdot \mathbf{d}_j], \\ \Gamma_{ij}^{\text{free,sc}}(\mathbf{r}_i, \mathbf{r}_j) &= 2\mu_0 \omega_0^2 \text{Im}[\mathbf{d}_i^* \cdot \bar{G}_{\text{free,sc}}(\mathbf{r}_i, \mathbf{r}_j, \omega_0) \cdot \mathbf{d}_j]. \end{aligned} \quad (6)$$

Results—We analyze the dynamics of the emitters, governed by the master equation (2). As illustrated in Fig. 1, we specify $x_1 - x_2 \equiv x$ and note that the two atoms are positioned at the same distance z from the surface. Consequently, in accordance with Eqs. (5) and (6), we can simplify the system by setting $\Omega_1^{(\mp)}(z) = \Omega_2^{(\mp)}(z) \equiv \Omega^{(\mp)}$, $\Omega_{12}^{(\mp)}(x, z) = \Omega_{21}^{(\mp)}(x, z) \equiv \Omega_{12}^{(\mp)}$, $\Gamma_{11}(z) = \Gamma_{22}(z) \equiv \Gamma$, and $\Gamma_{12}(x, z) = \Gamma_{21}(x, z) \equiv \Gamma_{12}$.

We introduce the atomic density matrix as $\hat{\rho}_S = \rho_{11} |ee\rangle \langle ee| + \rho_{22} |eg\rangle \langle eg| + \rho_{33} |ge\rangle \langle ge| + \rho_{23} |eg\rangle \langle ge| + \rho_{32} |ge\rangle \langle eg| + \rho_{44} |gg\rangle \langle gg|$. Considering the initial state of the two atoms as $\rho_S(t_0) = |eg\rangle \langle eg|$, the time-dependent elements of the density matrix can be obtained by solving the master equation (See SM)

$$\rho_{11}(t) = 0, \quad (7.1)$$

$$\rho_{44}(t) = 1 - \frac{1}{2} (e^{-(\Gamma - \Gamma_{12})t} + e^{-(\Gamma + \Gamma_{12})t}), \quad (7.2)$$

$$\Phi_+(t) = \frac{1}{2} (e^{-(\Gamma - \Gamma_{12})t} + e^{-(\Gamma + \Gamma_{12})t}), \quad (7.3)$$

$$\Phi_-(t) = \cos(2\Omega_{12}t) e^{-\Gamma t}, \quad (7.4)$$

$$\Psi_+(t) = -\frac{1}{2} (e^{-(\Gamma - \Gamma_{12})t} - e^{-(\Gamma + \Gamma_{12})t}), \quad (7.5)$$

$$\Psi_-(t) = i \sin(2\Omega_{12}t) e^{-\Gamma t} \quad (7.6)$$

Here, we define $\Phi_\pm \equiv \rho_{22} \pm \rho_{33}$ and $\Psi_\pm \equiv \rho_{23} \pm \rho_{32}$. According to Eqs. (7.1)–(7.6), all elements of the density matrix decay to zero as $t \rightarrow \infty$, except for ρ_{44}

(see Eq. (7.2)), which signifies both atoms being in their ground state, as expected. However, when $\Gamma = \Gamma_{12}$ (Eqs. (7.3)) and (7.5)), the system evolves to the steady state:

$$\rho_{\text{steady}} = \frac{1}{2} (|\psi_{\text{sub}}\rangle \langle \psi_{\text{sub}}| + |gg\rangle \langle gg|), \quad (8)$$

where $|\psi_{\text{sub}}\rangle \equiv (|eg\rangle - |ge\rangle) / \sqrt{2}$ corresponds to the sub-radiant state of the emitters that is decoupled from the EM field [55]. Thus we observe that quantum correlations emerge between the two emitters, transforming the initially uncorrelated state into an entangled steady state, with a concurrence of $C(\rho_{\text{steady}}) = 0.5$ [56].

The condition $\Gamma = \Gamma_{12}$ that yields the entangled steady-state signifies a balance between the emitters' spontaneous emission rate ($\Gamma = \Gamma_{11} = \Gamma_{22}$) and the surface-mediated dipole-dipole dissipative interaction (Γ_{12}), as was also analyzed in [38]. We introduce the relative decay $D(\mathbf{r}_1, \mathbf{r}_2) = \Gamma - \Gamma_{12}$, which is intricately dependent on the spatial arrangement of two emitters, their dipole orientation, and the properties of the surface. Initiating the system with one emitter in the excited state allows for the potential delocalization of a photon between the two emitters.

The steady-state entanglement condition thus corresponds to $D(\mathbf{r}_1, \mathbf{r}_2)$ approaching 0. We analyze two distinct dipole configurations, namely zz and xx (where atomic dipoles are perpendicular ($\theta = \pi/2$) and parallel ($\theta = 0$) to the surface, respectively (see Fig. 1)), and investigate the behavior of $D(\mathbf{r}_1, \mathbf{r}_2)$ as a function of the emitters' position.

The relative decay can be expressed as a sum of contributions from the free and scattering components: $D(\tilde{x}, \tilde{z}) = D^{\text{free}}(\tilde{x}) + D^{\text{sc}}(\tilde{x}, \tilde{z})$ where the scaled parameters are introduced as $\tilde{x} \equiv k_0 x$ and $\tilde{z} \equiv k_0 z$, with $k_0 = \omega_0/c$. The free part characterizes the system in the absence of the surface, while the scattering part accounts particularly for the surface effects. Utilizing Eq. (6), the free part is calculated as $D^{\text{free}}(\tilde{x}) = \Gamma_0 - \Gamma_{12}^{\text{free}}(\tilde{x})$. We note that the free part of the relative decay for both configurations as a function of \tilde{x} starts from zero and tends to Γ_0 for long distances, where the dipole-dipole interaction $\Gamma_{12}^{\text{free}}$ vanishes as the dipoles are infinitely separated from each other (see SM). The scattering part of the relative decay, besides \tilde{x} and dipole orientations, relies on \tilde{z} and the medium properties, defined as $D^{\text{sc}}(\tilde{x}, \tilde{z}) = \Gamma^{\text{sc}}(\tilde{x}, \tilde{z}) - \Gamma_{12}^{\text{sc}}(\tilde{x}, \tilde{z})$. First, we consider a perfect conductor surface with permittivity $\epsilon(\omega) \rightarrow \infty$, which is calculated for each dipole configuration based on Eq. (6). According to calculations, as \tilde{x} increases, the free and scattering components of the relative decay amplify each other in the zz configuration, leading to $D_{zz} \rightarrow 2\Gamma_0$, while in the xx configuration, their interaction is destructive, resulting in $D_{xx} \rightarrow 0$. The relative decay as a function of \tilde{x} is shown in Fig. 2 (a) for each dipole configura-

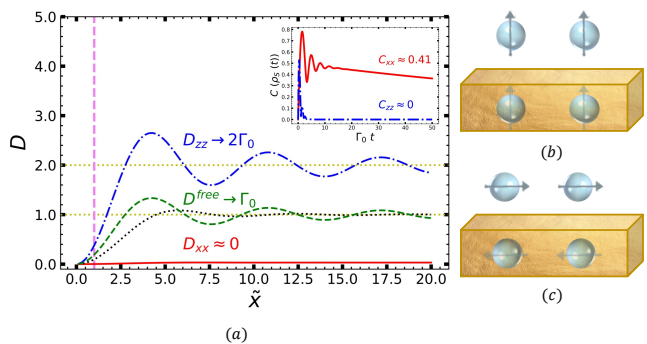


FIG. 2. (a) The relative decay in free space (green dashed and black dotted curves) and the total relative decay near the perfect conductor at a distance of $\tilde{z} = 0.2$, as functions of \tilde{x} for the zz (dash-dotted blue curve) and xx (solid red curve) configurations. The inset shows the density matrix's time-dependent concurrence for the system with zz (dash-dotted blue curve) and xx (solid red curve) configurations near the perfect conductor surface. (b) and (c), The schematic depicts the dipole-image model for the perpendicular dipoles in zz configuration and the parallel dipoles in xx configuration, along with their corresponding images in the medium.

tion: in free space, denoted by $D_{zz}^{\text{free}}(\tilde{x})$ and $D_{xx}^{\text{free}}(\tilde{x})$, and in the presence of a perfect conductor surface, considering the constant distance $\tilde{z} = 0.2$ from the surface, denoted by $D_{zz}^{\text{per}}(\tilde{x}, \tilde{z} = 0.2)$ and $D_{xx}^{\text{per}}(\tilde{x}, \tilde{z} = 0.2)$. It illustrates how the presence of the surface can assist with maintaining the relative decay close to zero when the dipoles are oriented parallel to the surface in the xx configuration. In the inset of Fig. 3 (a), we plot the time evolution of the concurrence between two emitters at the specific point ($\tilde{x} = 1, \tilde{z} = 0.2$), marked with the vertical dashed line in Fig. 3 (a), calculated based on the master equation (2). The emitters are assumed to be silicon-vacancy (SiV) centers embedded in a bulk diamond, placed near a surface with a transition wavelength $\lambda = 2\pi/k_0 = 737$ nm [57]. It indicates that the generated entanglement for the xx configuration, with $D_{xx}^{\text{per}} \approx 0$ (solid red curve), is preserved for a long time, while for the zz configuration, with $D_{zz}^{\text{per}} > 0$ (dash-dotted blue curve), it decays to zero significantly faster.

The interaction between emitters and the surface can be elucidated by the dipole-image model, where the perfect conductor surface acts as a mirror for the dipoles [51], as depicted in Fig. 2(b-c).

In the case of zz configuration, where dipoles are perpendicular to the surface, dipoles' field and their image reinforce each other. This reinforcement leads to a decay rate that approaches $2\Gamma_0$. Conversely, in the xx configuration, where dipoles are oriented parallel to the surface, the dipole and its image fields tend to cancel each other out. Consequently, the emitters experience a nearly zero-field environment, resulting in minimal decay. In addition to the dipole-dipole interaction, each emitter is in-

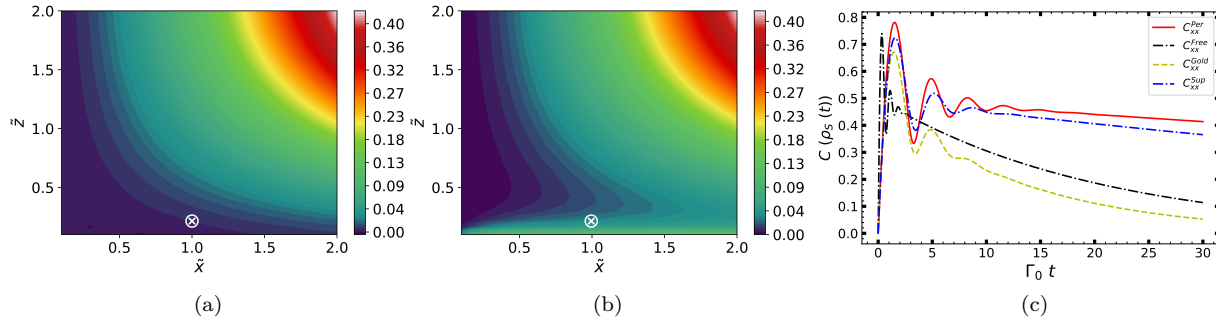


FIG. 3. Contour plot depicting $D(\tilde{x}, \tilde{z})$ in the vicinity of (a) superconducting, and (b) a gold surface where Zero relative decay is required for steady-state entanglement generation. (c) The evolution of concurrence between atoms over time for the xx configuration with $\tilde{x} = 1$ in free space (black dotted), and at a distance $\tilde{z} = 0.2$ from the perfect conductor (solid red), the superconducting (blue dash-dotted), and the gold surface (yellow dashed). However, atom-atom entanglement can persist for a long time even if the relative decay does not vanish completely. The selected position ($\tilde{x} = 1, \tilde{z} = 0.2$) is indicated by the white \otimes sign in contour plots.

fluenced by the other's image. These interactions result in a condition where the xx dipole configuration experiences almost no decay, highlighting how the surface effectively maintains the steady-state entanglement condition by minimizing the relative decay.

Focusing on xx configuration, we extend our analysis to a metal surface described by the Drude model and a superconducting surface. In this representation, we model the metal surface as gold, setting the plasma frequency to $\omega_p \approx 1.37 \times 10^{16}$ Hz and the loss parameter to $\gamma \approx 5.31 \times 10^{13}$ Hz [58] where the permittivity described as $\epsilon_d(\omega) = 1 - \omega_p^2/(\omega^2 + i\omega\gamma)$ [59]. Moreover, the permittivity for a London superconductor is given by [60]

$$\epsilon_s(\omega) = 1 - \frac{c^2}{\omega^2 \lambda_L^2(T)} + i \frac{2c^2}{\omega^2 \delta_L^2(T)} \quad (9)$$

The (square of the) London penetration length and the skin depth are defined as $\lambda_L^2(T) = \lambda_L^2(0)/[1 - (T/T_c)^4]$, and $\delta_L^2(T) = 2/(\omega\mu_0\sigma(T/T_c)^4)$, where $\sigma = 2 \times 10^9 \Omega^{-1}$ represents the electrical conductivity. We consider a superconducting Niobium with the critical temperature $T_c = 8.31$ K and $\lambda_L(0) = 35$ nm at a finite temperature $T = 0.01T_c$.

Fig. 3 (a-b) displays contour plots of $D(x, z)$ near (a) a Niobium superconductor, and (b) a gold surface, as functions of \tilde{x} and \tilde{z} . The transition from dark blue to red indicates an increase in relative decay from zero, with dark blue areas highlighting the parameter space where the steady-state or near steady-state entanglement condition is satisfied. According to Fig. 3(a), the relative decay tends to zero as the distance \tilde{z} from the surface decreases. For the superconducting surface in the non-retarded regime, $D_{xx}^{\text{Sup}} \propto (T/T_c)^4$ (See SM). Therefore, at low temperatures $T \ll T_c$, the relative decay is similar to that of a perfect conductor. In contrast, Fig. 3(b) shows that the relative decay increases as \tilde{z} decreases near

the gold surface. In the non-retarded regime ($\tilde{z} \ll 1$), it can be shown that $D_{xx}^{\text{Gold, sc}}(\tilde{x}, \tilde{z}) \propto \gamma\Gamma_0/\tilde{z}^3$. This demonstrates that in metals with non-zero loss, the emitters experience a noisier environment in the non-retarded regime as the distance from the metal surface decreases due to significant surface scattering. As illustrated in Fig. 3(b), an optimal distance from the surface can be determined to minimize the relative decay and maximize surface-mediated entanglement.

After analytically demonstrating the necessity of zero relative decay for steady-state entanglement generation, we numerically identified potential geometric configurations satisfying this condition in Fig. 3 (a)-(b). However, achieving exact zero relative decay may not be feasible in practice. Nonetheless, a significant amount of entanglement could still be maintained for an extended period between the emitters even if the relative decay does not vanish completely. According to our calculations, the relative decay of the system near a perfect conductor behaves similarly to that of the system near a superconducting surface (See SM). The relative decay for the superconducting surface (Fig. 3 (a)) can approach zero at $\tilde{z} \leq 0.2$, resulting in nearly steady-state entanglement, which can be further enhanced as \tilde{z} decreases. On the other hand, near the metal surface, the generated entanglement at $\tilde{z} < 0.2$ decays quickly due to near-field interactions. However, there is an optimal distance that minimizes the relative decay. For instance, the minimum value of the relative decay at $\tilde{x} = 1$ occurs at a distance of approximately $\tilde{z} \approx 0.4$ from the gold surface, resulting in maximum entanglement (Fig. 3 (b)). To compare different surfaces, we consider $\tilde{x} = 1$ ($x \approx 117$ nm) and $\tilde{z} = 0.2$ ($z \approx 23$ nm) to examine the entanglement generation. The selected coordinate is marked in the contour plots (Fig. 3 (a)-(b)). Furthermore, we consider a system of two emitters in free space at a distance of $\tilde{x} = 1$

without the presence of a surface, which serves as a baseline for free space dipole-dipole entanglement generation. This allows us to separate and elucidate the effect of each surface.

At this point, the relative decay for each type of the surface is obtained as $D_{xx}^{\text{per}}(1,0.2) = 2.2 \times 10^{-3}$, $D_{xx}^{\text{Sup}}(1,0.2) = 4.7 \times 10^{-3}$, and $D_{xx}^{\text{Gold}}(1,0.2) = 0.037$. The time evolution of the concurrence ($C(\rho_S(t))$) between two emitters at this point, calculated based on the master equation (2), is plotted in Fig. 3 (c). The calculations reveal that at scaled time $\Gamma_0 t = 30$, the generated entanglement near the perfect conductor and superconducting surfaces is approximately $C_{xx}^{\text{per}} \approx 0.41$ and $C_{xx}^{\text{Sup}} \approx 0.37$, respectively, while it decays to $C_{xx}^{\text{Gold}} \approx 0.05$ near the gold surface, and for free space $C_{xx}^{\text{free}} \approx 0.1$. According to Fig. 3 (c), the concurrence is enhanced by the presence of the perfect conductor (solid red curve) and superconducting surface (dashed-dotted blue curve) compared to free-space (dotted black curve), while the gold surface (dashed yellow curve) reduces entanglement generation. However, it can be shown that at point $\tilde{z} = 0.4$, as an optimum distance from the surface, with the same $\tilde{x} = 1$ the gold surface can also contribute positively, resulting in $C_{xx}^{\text{Gold}} \approx 0.24 > C_{xx}^{\text{free}}$.

Conclusion – In conclusion, this letter introduced a method for generating steady-state entanglement by investigating the dynamics of a system with two emitters near a surface, considering the CP interaction. We analyzed the emergence of steady-state entanglement through an analytical solution of the master equation, emphasizing the necessary conditions for its realization. We introduced relative decay function $D(\mathbf{r}_1, \mathbf{r}_2) = \Gamma - \Gamma_{12}$ defined by spontaneous emission rates ($\Gamma \equiv \Gamma_{11} = \Gamma_{22}$) and surface-mediated dipole-dipole dissipative interaction ($\Gamma_{12} = \Gamma_{21}$). We demonstrated that achieving an entangled steady-state with a concurrence of $C(\rho_{\text{steady}}) = 0.5$ is possible when the relative decay, expressed as a function of the spatial positions of the emitters, their dipole orientations, and surface properties, equals zero ($D(\mathbf{r}_1, \mathbf{r}_2) = 0$). First, we revealed that to satisfy this condition in a surface-mediated process, the emitters' dipoles must be oriented parallel to the surface. Moreover, the surface's optical properties affect the relative decay as a function of the emitters' position. We demonstrated that the superconducting surface closely corresponds to the perfect conductor, maintaining the relative decay near zero. In contrast, due to the metal's loss parameter, the relative decay increases near a metal surface in the non-retarded limit, leading to a faster decay of the generated entanglement. However, we identified an optimal distance from the metal surface that enhances entanglement generation compared to free space and preserves it for a longer time.

Our results are pertinent to understanding entanglement dynamics in confined geometries and hold practical implications for quantum information processing proto-

cols in nanoscale systems. The proposed method also hints at potential applications in near-surface quantum metrology and sensing, where entanglement could play a role in enhancing precision measurements and sensing capabilities. Furthermore, entanglement generation and decoherence from quantum fluctuations are a subject of broader interest in QED and macroscopic quantum systems[61–68].

Acknowledgments— We gratefully acknowledge Stefan Scheel for bringing Ref. [38] to our attention after the completion of this work. This work was supported by the Scientific and Technological Research Council of Türkiye (TÜBİTAK) under Project Numbers 120F089 and 123F150. M. I., O. P., and Ö. M. thank TÜBİTAK for their support. K.S. acknowledges support from the National Science Foundation under Award No. PHY-2418249, by the John Templeton Foundation under Award No. 62422, and Army Research Office under Award No. W911NF2410080.

* mizadyari18@ku.edu.tr
 † onur.pusuluk@gmail.com
 ‡ kanu@arizona.edu
 § omustecap@ku.edu.tr

- [1] I. D'Amico and et al, Nanoscale quantum optics, *La Rivista del Nuovo Cimento* **42**, 153 (2019).
- [2] D. E. Chang, J. S. Douglas, A. González-Tudela, C.-L. Hung, and H. J. Kimble, Colloquium: Quantum matter built from nanoscopic lattices of atoms and photons, *Rev. Mod. Phys.* **90**, 031002 (2018).
- [3] S. D. Wang, M. Haas, and P. Narang, Quantum interfaces to the nanoscale, *ACS Nano* **15**, 7879 (2021).
- [4] O. O. Soykal and M. E. Flatté, Strong field interactions between a nanomagnet and a photonic cavity, *Phys. Rev. Lett.* **104**, 077202 (2010).
- [5] A. González-Tudela, A. Reiserer, J. García-Ripoll, and et al., Light-matter interactions in quantum nanophotonic devices, *Nat Rev Phys* **3**, 807 (2024).
- [6] W. Fang, B. Lin, G. xiang Li, and Y. Yang, Selective mode excitations and spontaneous emission engineering in quantum emitter-photonic structure coupled systems, *Opt. Express* **30**, 21103 (2022).
- [7] D. Chang, V. Vuletic, and M. Lukin, Quantum nonlinear optics - photon by photon, *Nature Photon* **8**, 685 (2014).
- [8] M. Gullans, D. E. Chang, F. H. L. Koppens, F. J. GarciaAbajo, and M. D. Lukin, Single-photon nonlinear optics with graphene plasmons, *Phys. Rev. Lett.* **111**, 247401 (2013).
- [9] J. Volz, M. Scheucher, C. Junge, and et al., Nonlinear π phase shift for single fibre-guided photons interacting with a single resonator-enhanced atom, *Nature Photon* **8**, 965 (2014).
- [10] A. Skjarow, H. Kübler, C. S. Adams, T. Pfau, R. Löw, and H. Alaeian, Purcell-enhanced dipolar interactions in nanostructures, *Phys. Rev. Res.* **4**, 023073 (2022).
- [11] A. Goban and et al, Atom–light interactions in photonic crystals, *Nature Communications* **5**, 3808 (2014).
- [12] J. D. Thompson and et al, Coupling a single trapped

- atom to a nanoscale optical cavity, *Science* **340**, 1202 (2013).
- [13] N. Rivera and I. Kaminer, Light–matter interactions with photonic quasiparticles, *Nature Reviews Physics* **2**, 538 (2020).
- [14] A. F. Kockum, A. Miranowicz, S. D. Liberato, and et al., Ultrastrong coupling between light and matter, *Nature Reviews Physics* **1**, 295 (2019).
- [15] J. Flick, N. Rivera, and P. Narang, Strong light-matter coupling in quantum chemistry and quantum photonics, *Nanophotonics* **7**, 1479 (2018).
- [16] P. Forn-Díaz, L. Lamata, E. Rico, J. Kono, and E. Solano, Ultrastrong coupling regimes of light-matter interaction, *Reviews of Modern Physics* **91**, 025005 (2019).
- [17] F. F. et al, Photonic quantum information processing: a review, *Reports on Progress in Physics* **82**, 016001 (2018).
- [18] A. Laucht and et al, Roadmap on quantum nanotechnologies, *Nanotechnology* **32**, 162003 (2021).
- [19] Y. Koo, T. Moon, M. Kang, and et al., Dynamical control of nanoscale light-matter interactions in low-dimensional quantum materials, *Light Sci Appl* **13**, 30 (2024).
- [20] G. B. et al, Ultrafast measurements of the dynamics of single nanostructures: a review, *Rep. Prog. Phys.* **82**, 016401 (2018).
- [21] J. Sánchez-Cánovas and M. Donaire, Nonconservative dipole forces on an excited two-atom system, *Phys. Rev. A* **106**, 032805 (2022).
- [22] H. B. G. Casimir and D. Polder, The influence of retardation on the london-van der waals forces, *Phys. Rev.* **73**, 360 (1948).
- [23] B. Dutta, J. C. Carvalho, G. Garcia-Arellano, P. Pedri, A. Laliotis, C. Boldt, J. Kaushal, and S. Scheel, Effects of higher-order casimir-polder interactions on rydberg atom spectroscopy, *Phys. Rev. Res.* **6**, L022035 (2024).
- [24] G. L. Klimchitskaya, U. Mohideen, and V. M. Mostepanenko, The casimir force between real materials: Experiment and theory, *Rev. Mod. Phys.* **81**, 1827 (2009).
- [25] J. Sánchez-Cánovas and M. Donaire, Nonconservative dipole forces on an excited two-atom system, *Phys. Rev. A* **106**, 032805 (2022).
- [26] K. Sinha, B. P. Venkatesh, and P. Meystre, Collective effects in casimir-polder forces, *Phys. Rev. Lett* **121**, 183605 (2018).
- [27] D. Hümmer, P. Schneeweiss, A. Rauschenbeutel, and O. Romero-Isart, Heating in nanophotonic traps for cold atoms, *Phys. Rev. X* **9**, 041034 (2019).
- [28] C. Henkel and M. Wilkens, Heating of trapped atoms near thermal surfaces, *Europhysics Letters* **47**, 414 (1999).
- [29] A. G. J. MacFarlane, J. P. Dowling, and G. J. Milburn, Quantum technology: the second quantum revolution, *Philosophical Transactions of the Royal Society of London. Series A: Mathematical, Physical and Engineering Sciences* **361**, 1655 (2003).
- [30] I. H. Deutsch, Harnessing the power of the second quantum revolution, *PRX Quantum* **1**, 020101 (2020).
- [31] R. E. Evans and et al, Photon-mediated interactions between quantum emitters in a diamond nanocavity, *Science* **362**, 662 (2018).
- [32] M. D. Lukin and P. R. Hemmer, Quantum entanglement via optical control of atom-atom interactions, *Phys. Rev. Lett.* **84**, 2818 (2000).
- [33] T. Neuman, M. Trusheim, and P. Narang, Selective acoustic control of photon-mediated qubit-qubit interactions, *Phys. Rev. A* **101**, 052342 (2020).
- [34] A. Laucht and et al, Electrical control of spontaneous emission and strong coupling for a single quantum dot, *New Journal of Physics* **11**, 023034 (2009).
- [35] D. Braun, Creation of entanglement by interaction with a common heat bath, *Phys. Rev. Lett.* **89**, 277901 (2002).
- [36] F. Benatti, R. Floreanini, and M. Piani, Environment induced entanglement in markovian dissipative dynamics, *Phys. Rev. Lett.* **91**, 070402 (2003).
- [37] M. Cattaneo, G. L. Giorgi, S. Maniscalco, G. S. Paraoanu, and R. Zambrini, Bath-induced collective phenomena on superconducting qubits: Synchronization, subradiance, and entanglement generation, *Annalen der Physik* **533**, 2100038 (2021), <https://onlinelibrary.wiley.com/doi/pdf/10.1002/andp.202100038>.
- [38] H. T. Dung, S. Scheel, D.-G. Welsch, and L. Knöll, Atomic entanglement near a realistic microsphere, *Journal of Optics B: Quantum and Semiclassical Optics* **4**, S169 (2002).
- [39] E. Amooghorban and E. Alebrahim, Entanglement dynamics of two two-level atoms in the vicinity of an invisibility cloak, *Phys. Rev. A* **96**, 012339 (2017).
- [40] M. Brownnutt, M. Kumph, P. Rabl, and R. Blatt, Ion-trap measurements of electric-field noise near surfaces, *Rev. Mod. Phys.* **87**, 1419 (2015).
- [41] C. Wang, C. Axline, Y. Y. Gao, T. Brecht, Y. Chu, L. Frunzio, M. H. Devoret, and R. J. Schoelkopf, Surface participation and dielectric loss in superconducting qubits, *Applied Physics Letters* **107**, 162601 (2015).
- [42] M. Kim, H. J. Mamin, M. H. Sherwood, K. Ohno, D. D. Awschalom, and D. Rugar, Decoherence of near-surface nitrogen-vacancy centers due to electric field noise, *Phys. Rev. Lett.* **115**, 087602 (2015).
- [43] P. Jamonneau and et al, Competition between electric field and magnetic field noise in the decoherence of a single spin in diamond, *Phys. Rev. B* **93**, 024305 (2016).
- [44] Y. Yang, C. Callegari, X. Feng, and M. Roukes, Surface adsorbate fluctuations and noise in nanoelectromechanical systems, *Nano letters* **11**, 1753 (2011).
- [45] D. Reiche, K. Busch, and F. Intravaia, Nonadditive enhancement of nonequilibrium atom-surface interactions, *Phys. Rev. Lett.* **124**, 193603 (2020).
- [46] K. Jain, L. Ruks, F. le Kien, and T. Busch, Strong dipole-dipole interactions via enhanced light-matter coupling in composite nanofiber waveguides, e-print arXiv:2405.06168 [quant-ph] (2024).
- [47] M. Donaire and A. Lambrecht, Coherent effect of vacuum fluctuations on driven atoms, *Phys. Rev. A* **92**, 013838 (2015).
- [48] M. Donaire, M. Gorza, A. Maury, R. Guerout, and A. Lambrecht, Casimir-polder-induced rabi oscillations, *Europhysics Letters* **109**, 24003 (2015).
- [49] S. Scheel and S. Y. Buhmann, Macroscopic qed - concepts and applications (2009), arXiv:0902.3586 [quant-ph].
- [50] D. E. Chang, K. Sinha, J. M. Taylor, and H. J. Kimble, Trapping atoms using nanoscale quantum vacuum forces, *Nat Commun* **5**, 4343 (2014).
- [51] S. Y. Buhmann, *Dispersion Forces I* (Springer-Verlag, Berlin, 2012).
- [52] H.-P. Breuer and F. Petruccione, *Theory of Open Quantum Systems* (Oxford University Press, New York, 2002).
- [53] A. Olivera, K. Sinha, and P. Solano, Dipole-dipole inter-

- actions through a lens, *Phys. Rev. A* **106**, 013703 (2022).
- [54] A. Sone, K. Sinha, and S. Deffner, Thermodynamic perspective on quantum fluctuations, e-print arXiv:2308.04951 [cond-mat.stat-mech] (2024).
- [55] R. H. Dicke, Coherence in spontaneous radiation processes, *Phys. Rev.* **93**, 99 (1954).
- [56] R. Horodecki, P. Horodecki, M. Horodecki, and K. Horodecki, Quantum entanglement, *Rev. Mod. Phys.* **81**, 865 (2009).
- [57] Y. Zhou, A. Rasmita, K. Li, and et al., Coherent control of a strongly driven silicon vacancy optical transition in diamond, *Nature Photon* **8**, 14451 (2017).
- [58] I. Pirozhenko, A. Lambrecht, and V. B. Svetovoy, Sample dependence of the casimir force, *New Journal of Physics* **8**, 238 (2006).
- [59] J. D. Jackson, *Classical electrodynamics* (Wiley, New York, 1999).
- [60] B.-S. Skagerstam, U. Hohenester, A. Eiguren, and P. K. Rekdal, Spin decoherence in superconducting atom chips, *Phys. Rev. Lett.* **97**, 070401 (2006).
- [61] S. Bose, A. Mazumdar, G. W. Morley, H. Ulbricht, M. Toroš, M. Paternostro, A. A. Geraci, P. F. Barker, M. S. Kim, and G. Milburn, Spin entanglement witness for quantum gravity, *Phys. Rev. Lett.* **119**, 240401 (2017).
- [62] T. W. van de Kamp, R. J. Marshman, S. Bose, and A. Mazumdar, Quantum gravity witness via entanglement of masses: Casimir screening, *Phys. Rev. A* **102**, 062807 (2020).
- [63] C. Marletto and V. Vedral, Gravitationally induced entanglement between two massive particles is sufficient evidence of quantum effects in gravity, *Phys. Rev. Lett.* **119**, 240402 (2017).
- [64] K. Sinha and Y. Subasi, Quantum brownian motion of a particle from casimir-polder interactions, *Phys. Rev. A* **101**, 032507 (2020).
- [65] L. Martinetz, K. Hornberger, and B. A. Stickler, Surface-induced decoherence and heating of charged particles, *PRX Quantum* **3**, 030327 (2022).
- [66] F. M. D'Angelis, F. A. Pinheiro, and F. Impens, Decoherence and collective effects of quantum emitters near a medium at criticality, *Phys. Rev. B* **99**, 195451 (2019).
- [67] S. Fedida and A. Serafini, Tree-level entanglement in quantum electrodynamics, *Phys. Rev. D* **107**, 116007 (2023).
- [68] S. Cheng, H. Yu, and J. Hu, Quantum fluctuations of spacetime generate quantum entanglement between gravitationally polarizable subsystems, *Eur. Phys. J. C* **78**, 954 (2018).

Supplemental material for "Steady-state Entanglement Generation via Casimir-Polder Interaction"

Mohsen Izadyari,^{1,2,*} Onur Pusuluk,^{2,†} Kanu Sinha,^{3,‡} and Özgür E. Müstecaphoğlu^{1,4,5,§}

¹*Department of Physics, Koç University, 34450 Sarıyer, Istanbul, Türkiye*

²*Faculty of Engineering and Natural Sciences, Kadir Has University, 34083 Fatih, Istanbul, Türkiye*

³*College of Optical Sciences and Department of Physics,
University of Arizona, Tucson, AZ, 85721, USA*

⁴*TÜBİTAK Research Institute for Fundamental Sciences, 41470 Gebze, Türkiye*

⁵*Faculty of Engineering and Natural Sciences, Sabanci University, 34956 Tuzla, Istanbul, Türkiye*

SURFACE-MEDIATED VACUUM ELECTROMAGNETIC FIELD

The Hamiltonian for the vacuum EM field near a surface in macroscopic QED formalism is written as

$$\hat{H}_F = \sum_{\lambda=e,m} \int d^3\mathbf{r}' \int d\omega \hbar\omega \hat{f}_\lambda^\dagger(\mathbf{r},\omega) \cdot \hat{f}_\lambda(\mathbf{r},\omega). \quad (1)$$

Here, $\hat{f}_\lambda(\mathbf{r},\omega)$ and $\hat{f}_\lambda^\dagger(\mathbf{r},\omega)$ are the bosonic annihilation and creation operators in the presence of the medium, as defined in the main text. They follow the canonical commutation relations $[\hat{f}_\lambda(\mathbf{r},\omega), \hat{f}_\lambda^\dagger(\mathbf{r}',\omega)] = \delta_{\lambda\lambda'} \delta(\mathbf{r}-\mathbf{r}') \delta(\omega-\omega')$.

The electric field operator at position \mathbf{r} is given by Eq. (1) in the main text, wherein the coefficients $\bar{\mathbf{G}}_\lambda(\mathbf{r},\mathbf{r}',\omega)$ defined by

$$\begin{aligned} \bar{\mathbf{G}}_e(\mathbf{r},\mathbf{r}',\omega) &= i \frac{\omega^2}{c^2} \sqrt{\frac{\hbar}{\pi\epsilon_0} \text{Im}[\epsilon(\mathbf{r}',\omega)]} \bar{\mathbf{G}}(\mathbf{r},\mathbf{r}',\omega), \\ \bar{\mathbf{G}}_m(\mathbf{r},\mathbf{r}',\omega) &= i \frac{\omega^2}{c^2} \sqrt{\frac{\hbar}{\pi\epsilon_0} \frac{\text{Im}[\mu(\mathbf{r}',\omega)]}{|\mu(\mathbf{r}',\omega)|^2}} \nabla \times \bar{\mathbf{G}}(\mathbf{r},\mathbf{r}',\omega). \end{aligned} \quad (2)$$

where the Green's tensor satisfies the inhomogeneous Helmholtz equation in the presence of the medium as follow

$$\nabla \times \nabla \times \bar{\mathbf{G}}(\mathbf{r},\mathbf{r}',\omega) - \epsilon(\mathbf{r},\omega) \frac{\omega^2}{c^2} \bar{\mathbf{G}}(\mathbf{r},\mathbf{r}',\omega) = \delta(\mathbf{r}-\mathbf{r}'), \quad (3)$$

where $\bar{\mathbf{G}}(\mathbf{r},\mathbf{r}',\omega) = \bar{\mathbf{G}}_{\text{free}}(\mathbf{r},\mathbf{r}',\omega) + \bar{\mathbf{G}}_{\text{sc}}(\mathbf{r},\mathbf{r}',\omega)$ incorporates the free space and scattering components of the total Green's tensor. The permittivity and permeability of the medium are denoted by $\epsilon(\mathbf{r},\omega)$, and $\mu(\mathbf{r},\omega)$, respectively.

Considering a dipole near an infinite half-space surface located at point \mathbf{r}_1 , the scattering Green's tensor is obtained as:

$$\begin{aligned} \bar{\mathbf{G}}_{\text{sc}}(x,z,\omega) &= \frac{i}{8\pi} \int_0^\infty dk_\parallel \frac{k_\parallel}{k_\perp} e^{2ik_\perp z} \left[\begin{pmatrix} J_0(k_\parallel x) + J_2(k_\parallel x) & 0 & 0 \\ 0 & J_0(k_\parallel x) - J_2(k_\parallel x) & 0 \\ 0 & 0 & 0 \end{pmatrix} r_s \right. \\ &\quad \left. + \frac{c^2}{\omega^2} \begin{pmatrix} -k_\perp^2 [J_0(k_\parallel x) - J_2(k_\parallel x)] & 0 & -2ik_\parallel k_\perp J_0(k_\parallel x) \\ 0 & -k_\perp^2 [J_0(k_\parallel x) + J_2(k_\parallel x)] & 0 \\ 2ik_\parallel k_\perp J_0(k_\parallel x) & 0 & 2k_\parallel^2 J_0(k_\parallel x) \end{pmatrix} r_p \right] \end{aligned} \quad (4)$$

Here, we consider $|\mathbf{r}_1 - \mathbf{r}_2| = x$ and $(\mathbf{r}_1 + \mathbf{r}_2) \cdot \hat{z} = z$. The Fresnel coefficients for s - and p -polarized light reflecting from the surface are denoted as $r_s = \frac{k_\perp - k_\perp^1}{k_\perp + k_\perp^1}$ and $r_p = \frac{\epsilon(\omega)k_\perp - k_\perp^1}{\epsilon(\omega)k_\perp + k_\perp^1}$, respectively, where $k_\perp^2 = \omega^2 - k_\parallel^2$, where $k_\perp^1 = \sqrt{\epsilon(\omega)\omega^2/c^2 + k_\parallel^2}$.

Moreover, the free Green's tensor between \mathbf{r}_1 , and \mathbf{r}_2 gives

$$\bar{\mathbf{G}}_{\text{free}}(\mathbf{r}_1, \mathbf{r}_2, \omega) = -\frac{c^2 e^{i\omega x/c}}{4\pi\omega^2 x^3} \begin{pmatrix} g(-i\omega x/c) - h(-i\omega x/c) & 0 & 0 \\ 0 & g(-i\omega x/c) & 0 \\ 0 & 0 & g(-i\omega x/c) \end{pmatrix} \quad (5)$$

STEADY-STATE CALCULATIONS

The equations of the motion for the density matrix elements can be obtained from the master equation (Eq. 2 in the main text) as follows:

$$\frac{d\rho_{11}(t)}{dt} = -2\Gamma \rho_{11}(t) \quad (6.1)$$

$$\frac{d\rho_{44}(t)}{dt} = \Gamma \left(\rho_{22}(t) + \rho_{33}(t) \right) + \Gamma_{12} \left(\rho_{23}(t) + \rho_{32}(t) \right) \quad (6.2)$$

$$\frac{d\rho_{22}(t)}{dt} = -\frac{i}{\hbar}\Omega_{12} \left(\rho_{32}(t) - \rho_{23}(t) \right) + \Gamma \left(\rho_{11}(t) - \rho_{22}(t) \right) - \frac{\Gamma_{12}}{2} \left(\rho_{23}(t) + \rho_{32}(t) \right) \quad (6.3)$$

$$\frac{d\rho_{33}(t)}{dt} = -\frac{i}{\hbar}\Omega_{12} \left(\rho_{23}(t) - \rho_{32}(t) \right) + \Gamma \left(\rho_{11}(t) - \rho_{33}(t) \right) - \frac{\Gamma_{12}}{2} \left(\rho_{23}(t) + \rho_{32}(t) \right) \quad (6.4)$$

$$\frac{d\rho_{23}(t)}{dt} = -\frac{i}{\hbar}\Omega_{12} \left(\rho_{33}(t) - \rho_{22}(t) \right) - \Gamma \rho_{23}(t) + \frac{\Gamma_{12}}{2} \left(2\rho_{11}(t) - \rho_{22}(t) - \rho_{33}(t) \right) \quad (6.5)$$

$$\frac{d\rho_{32}(t)}{dt} = -\frac{i}{\hbar}\Omega_{12} \left(\rho_{22}(t) - \rho_{33}(t) \right) - \Gamma \rho_{32}(t) + \frac{\Gamma_{12}}{2} \left(2\rho_{11}(t) - \rho_{22}(t) - \rho_{33}(t) \right) \quad (6.6)$$

Considering initial state $|\psi_0(t=0)\rangle = |eg\rangle$, the solution of the equation of the motion is obtained as shown in Eqs. (8.1)-(8.6) in the main text where the steady state can be obtained in the limit $t \rightarrow \infty$ as

$$\begin{aligned} \rho_{steady} &= \frac{1}{2} |gg\rangle \langle gg| + \frac{1}{2} \left[\left(|eg\rangle \langle eg| + |ge\rangle \langle ge| \right) - \left(|eg\rangle \langle ge| + |ge\rangle \langle eg| \right) \right] \\ &= \frac{1}{2} \left(|gg\rangle \langle gg| + |\psi_{sub}\rangle \langle \psi_{sub}| \right) \end{aligned} \quad (7)$$

Here, $|\psi_{sub}\rangle = (|eg\rangle - |ge\rangle)/\sqrt{2}$.

RELATIVE DECAY

The relative decay is written as free and scattering components' contributions

$$D(\tilde{x}, \tilde{z}) = D^{free}(\tilde{x}) + D^{sc}(\tilde{x}, \tilde{z}), \quad (8)$$

where $D^{free}(\tilde{x}) = \Gamma_0 - \Gamma_{12}^{free}(\tilde{x})$, for zz and xx dipole configurations is calculated as

$$\begin{aligned} D_{zz}^{free}(\tilde{x}) &= \Gamma_0 - \frac{2\mu_0\omega_0^2|d|^2}{\hbar} \text{Im}[\mathbf{z} \cdot (\bar{G}_{free}(\mathbf{r}_1, \mathbf{r}_2, \omega_0)) \cdot \mathbf{z}] \\ &= \Gamma_0 + \frac{3\Gamma_0}{2\tilde{x}^3} \left((1 - \tilde{x}^2) \sin(\tilde{x}) - \tilde{x} \cos(\tilde{x}) \right) \end{aligned} \quad (9)$$

$$\begin{aligned} \Gamma_{12}^{free,xx}(\tilde{x}) &= \Gamma_0 - \frac{2\mu_0\omega_0^2|d|^2}{\hbar} \text{Im}[\mathbf{x} \cdot (\bar{G}_{free}(\mathbf{r}_1, \mathbf{r}_2, \omega_0)) \cdot \mathbf{x}] \\ &= \Gamma_0 - \frac{3\Gamma_0}{\tilde{x}^3} \left(\sin(\tilde{x}) - \tilde{x} \cos(\tilde{x}) \right), \end{aligned} \quad (10)$$

and the scattering part $D^{sc}(\tilde{x}, \tilde{z}) = \Gamma_{11}^{sc}(\tilde{z}) - \Gamma_{12}^{sc}(\tilde{x}, \tilde{z})$.

For zz dipole configuration, we have

$$\Gamma_{11}^{sc,zz}(\tilde{z}) = \frac{3\Gamma_0}{8\tilde{z}^3} \left((\sin(2\tilde{z}) - 2\tilde{z} \cos(2\tilde{z})) \text{Re}[r_p] + (2\tilde{z} \sin(2\tilde{z}) + \cos(2\tilde{z})) \text{Im}[r_p] \right) \quad (11)$$

$$\Gamma_{12}^{sc,zz}(\tilde{x}, \tilde{z}) = \frac{3\Gamma_0}{2} \left(\int_0^1 d\tilde{k}_\perp (1 - \tilde{k}_\perp^2) J_0(\tilde{x} \sqrt{1 - \tilde{k}_\perp^2}) (\cos(2\tilde{k}_\perp \tilde{z}) \text{Re}[r_p] - \sin(2\tilde{k}_\perp \tilde{z}) \text{Im}[r_p]) \right)$$

$$+ \int_0^\infty d\tilde{\kappa}_\perp e^{-2\tilde{\kappa}_\perp \tilde{z}} (1 + \tilde{\kappa}_\perp^2) J_0(\tilde{x} \sqrt{1 + \tilde{\kappa}_\perp^2}) \text{Im}[r_p], \quad (12)$$

and for xx configuration

$$\Gamma_{11}^{\text{sc},xx}(\tilde{z}) = -\frac{3\Gamma_0}{16\tilde{z}^3} \left((2\tilde{z} \cos(2\tilde{z}) + (2\tilde{z}^2 - 1) \sin(2\tilde{z})) \text{Re}[r_p] - (2\tilde{z} \sin(2\tilde{z}) + (1 - 2\tilde{z}^2) \cos(2\tilde{z})) \text{Im}[r_p] \right) \quad (13)$$

$$\begin{aligned} \Gamma_{12}^{\text{sc},xx}(\tilde{x}, \tilde{z}) = & -\frac{3\Gamma_0}{4} \left(\int_0^1 d\tilde{k}_\perp \tilde{k}_\perp^2 (J_0(\tilde{x} \sqrt{1 - \tilde{k}_\perp^2}) - J_2(\tilde{x} \sqrt{1 - \tilde{k}_\perp^2})) (\cos(2\tilde{k}_\perp \tilde{z}) \text{Re}[r_p] - \sin(2\tilde{k}_\perp \tilde{z}) \text{Im}[r_p]) \right. \\ & \left. - \int_0^\infty d\tilde{\kappa}_\perp e^{-2\tilde{\kappa}_\perp \tilde{z}} \tilde{\kappa}_\perp^2 (J_0(\tilde{x} \sqrt{1 + \tilde{\kappa}_\perp^2}) - J_2(\tilde{x} \sqrt{1 + \tilde{\kappa}_\perp^2})) \text{Im}[r_p] \right) \end{aligned} \quad (14)$$

In the following, we describe three different surfaces with different permittivities.

Perfect Conductor

In a perfect conductor $\epsilon(\omega) \rightarrow \infty$, and as a results the Fresnel coefficients become

$$\begin{aligned} r_s^{\text{Per}} &= -1 \\ r_p^{\text{Per}} &= 1 \end{aligned} \quad (15)$$

Accordingly, it can be calculated

$$\Gamma_{11}^{\text{sc},zz}(\tilde{z}) = \frac{3\Gamma_0}{8\tilde{z}^3} (\sin(2\tilde{z}) - 2\tilde{z} \cos(2\tilde{z})) \quad (16)$$

$$\Gamma_{12}^{\text{sc},zz}(\tilde{x}, \tilde{z}) = \frac{3\Gamma_0}{2} \left(\int_0^1 d\tilde{k}_\perp (1 - \tilde{k}_\perp^2) J_0(\tilde{x} \sqrt{1 - \tilde{k}_\perp^2}) \cos(2\tilde{k}_\perp \tilde{z}) \right), \quad (17)$$

$$\Gamma_{11}^{\text{sc},xx}(\tilde{z}) = -\frac{3\Gamma_0}{16\tilde{z}^3} (2\tilde{z} \cos(2\tilde{z}) + (2\tilde{z}^2 - 1) \sin(2\tilde{z})) \quad (18)$$

$$\Gamma_{12}^{\text{sc},xx}(\tilde{x}, \tilde{z}) = -\frac{3\Gamma_0}{4} \left(\int_0^1 d\tilde{k}_\perp \tilde{k}_\perp^2 (J_0(\tilde{x} \sqrt{1 - \tilde{k}_\perp^2}) - J_2(\tilde{x} \sqrt{1 - \tilde{k}_\perp^2})) (\cos(2\tilde{k}_\perp \tilde{z})) \right) \quad (19)$$

The decay function, defined by $\Gamma(\tilde{z}) = \Gamma_0 + \Gamma^{\text{sc}}(\tilde{z})$, is plotted in Fig. 1 as a function of \tilde{z} for an emitter with perpendicular (zz) and parallel (xx) dipole orientations. According to Eqs. (16) and (18), in the non-retarded regime where $\tilde{z} \ll 1$, it can be observed that $\Gamma_{11}^{\text{sc},zz} \rightarrow \Gamma_0$, while $\Gamma_{11}^{\text{sc},xx} \rightarrow -\Gamma_0$. Consequently, in the non-retarded limit, $\Gamma \rightarrow 2\Gamma_0$ and $\Gamma \rightarrow 0$. As \tilde{z} increases, it tends to Γ_0 , which diminishes the surface's effect, as shown in Fig. 1 (a). The scattering part of the relative decay near a perfect conductor is calculated for each dipole configuration based on Eq. (7) in the main text as

$$\begin{aligned} D_{zz}^{\text{sc,per}}(\tilde{x}, \tilde{z}) &= \frac{3\Gamma_0}{2} \left[\frac{\sin(2\tilde{z}) - 2\tilde{z} \cos(2\tilde{z})}{4\tilde{z}^3} - \mathcal{G}_{zz}(\tilde{x}, \tilde{z}) \right] \\ D_{xx}^{\text{sc,per}}(\tilde{x}, \tilde{z}) &= -\frac{3\Gamma_0}{4} \left[\frac{(4\tilde{z}^2 - 1) \sin(2\tilde{z}) + 2\tilde{z} \cos(2\tilde{z})}{4\tilde{z}^3} - \mathcal{G}_{xx}(\tilde{x}, \tilde{z}) \right]. \end{aligned} \quad (20)$$

Here we have introduced

$$\begin{aligned} \mathcal{G}_{zz}(\tilde{x}, \tilde{z}) &\equiv \int_0^1 d\tilde{k}_\perp \cos(2\tilde{k}_\perp \tilde{z}) (1 - \tilde{k}_\perp^2) J_0(\tilde{k}_\parallel \tilde{x}) \\ \mathcal{G}_{xx}(\tilde{x}, \tilde{z}) &\equiv \int_0^1 d\tilde{k}_\perp \cos(2\tilde{k}_\perp \tilde{z}) ([J_0(\tilde{k}_\parallel \tilde{x}) + J_2(\tilde{k}_\parallel \tilde{x})] - \tilde{k}_\perp^2 [J_0(\tilde{k}_\parallel \tilde{x}) - J_2(\tilde{k}_\parallel \tilde{x})]), \end{aligned} \quad (21)$$

where $\tilde{k}_\parallel = \sqrt{1 - \tilde{k}_\perp^2}$. Furthermore, we calculate the relative decay as a function of \tilde{x} in the non-retarded limit, where the emitters are assumed to be at a constant distance \tilde{z} from the surface, and plot it for two dipole configurations in Fig. 1(b). The figure shows that in the xx configuration, the relative decay remains close to zero, while in the zz configuration, it increases as \tilde{x} increases.

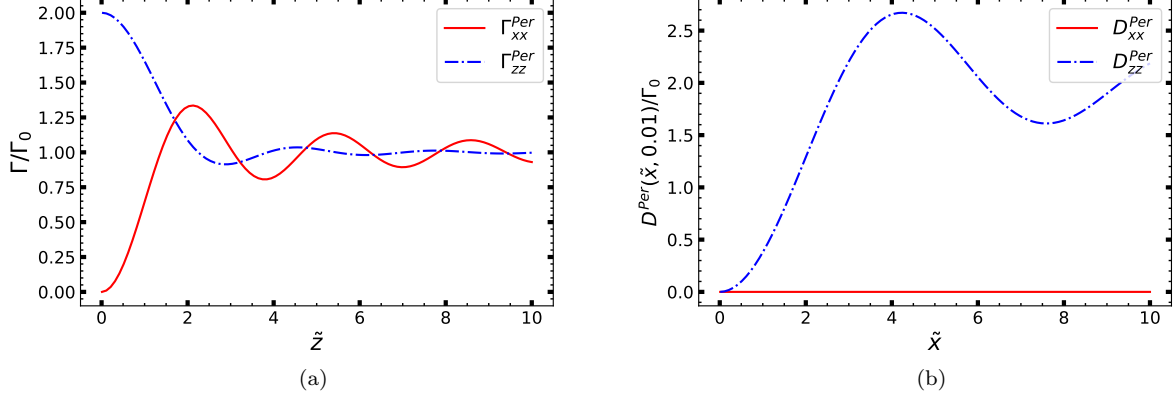


FIG. 1. (a) The single emitter decay $\Gamma(\tilde{z})$ as a function of \tilde{z} and (b) The relative decay $D(\tilde{x}, \tilde{z})$ as a function of \tilde{x} where $\tilde{z} = 0.01$ for xx (the solid red curve), and zz (dashed blue curve) configurations near a perfect conductor.

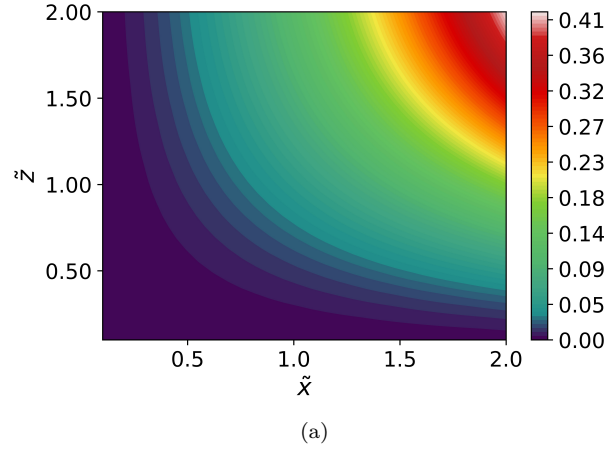


FIG. 2. The contour plot of the relative decay as a function of \tilde{x} , and \tilde{z} near a perfect conducting surface for xx configuration.

Drude Model (Metal Surface)

The Drude model describes the permittivity of a metal surface as follows:

$$\epsilon(\omega) = 1 - \frac{\omega_p^2}{\omega^2 + i\omega\gamma}, \quad (22)$$

where ω_p and γ describe the plasma frequency and loss parameter of the medium.

In non-retarded limit, it can be supposed that $k_{\perp}^1 = \sqrt{\epsilon(\omega)\omega^2/c^2 + k_{\parallel}^2} \approx k_{\perp}$, the Fresnel coefficients can be thus approximated as:

$$\begin{aligned} r_s &= \frac{k_{\perp} - k_{\perp}^1}{k_{\perp} + k_{\perp}^1} \approx 0 \\ r_p &= \frac{\epsilon(\omega)k_{\perp} - k_{\perp}^1}{\epsilon(\omega)k_{\perp} + k_{\perp}^1} \approx \frac{\epsilon(\omega) - 1}{\epsilon(\omega) + 1} \approx \frac{-\omega_p^2}{(2\omega^2 - \omega_p^2) + 2i\omega\gamma} \end{aligned} \quad (23)$$

As a result, the relative decay for xx configuration is given

$$D_{xx}^{Drude}(\tilde{x}, \tilde{z}) = \left[\left(1 - \frac{3(\sin(\tilde{x}) - \tilde{x}\cos(\tilde{x}))}{\tilde{x}^3} \right) + \frac{3}{8} \left(\frac{\omega\gamma}{\omega_p^2} \right) \left(\frac{1}{\tilde{z}^3} - 4\mathcal{F}_{xx}(\tilde{x}, \tilde{z}) \right) \right] \Gamma_0 \quad (24)$$

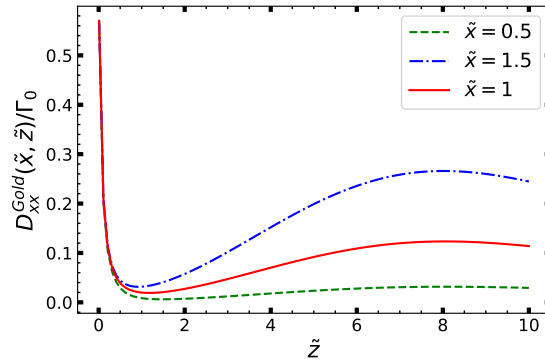


FIG. 3. The relative decay $D(\tilde{x}, \tilde{z})$ as a function of \tilde{x} for $\tilde{z} = 0.5, 1, 1.5$ near a gold surface.

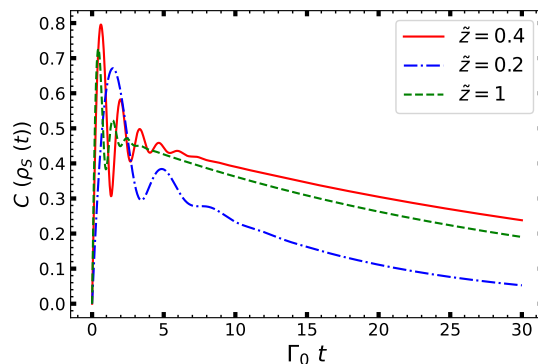


FIG. 4. Evolution of concurrence $C_{xx}^{Gold}(\tilde{x}, \tilde{z})$ vs. scaled time $\Gamma_0 t$ for a constant $\tilde{x} = 1$ and at distances $\tilde{z} = 0.2, 0.4, 1$ from the gold surface.

Here, we introduced

$$\mathcal{F}_{xx}(\tilde{x}, \tilde{z}) \equiv \int_0^\infty d\tilde{\kappa}_\perp e^{-2\tilde{\kappa}_\perp \tilde{z}} \tilde{\kappa}_\perp^2 (J_0(\tilde{\kappa}_\parallel \tilde{x}) - J_2(\tilde{\kappa}_\parallel \tilde{x})) \quad (25)$$

Unlike in a perfect conductor, in the non-retarded limit, $D_{xx}^{\text{Drude}} \propto \gamma \Gamma_0 / \tilde{z}^3$, indicating that the relative decay cannot be zero unless considering a lossless metal. We plot the relative decay in Fig. 3 for a gold surface using the Drude model, with a plasma frequency of $\omega_p \approx 1.37 \times 10^{16}$ Hz and a loss parameter of $\gamma \approx 5.31 \times 10^{13}$ Hz. Fig. 3 shows the relative decay as a function of \tilde{z} for three values of \tilde{x} : 0.5, 1, and 1.5. As discussed, the relative decay increases exponentially as \tilde{z} decreases. However, the figure also shows that there is an optimum distance from the surface that minimizes the relative decay, and this optimum distance varies for different values of \tilde{x} . In this regard, Fig. 4 indicates the time-dependent concurrence of the system for distances $\tilde{z} = 0.2, 0.4, 1$ while keeping $\tilde{x} = 1$ as the constant distance between emitters. As it shows, at $\tilde{z} = 0.4$, where $D_{xx}^{Gold}(\tilde{x} = 1, \tilde{z})$ is minimum, the generated entanglement is maximum, and at time $\Gamma_0 t = 30$ it gives $C_{xx}^{Gold} \approx 0.24$. It thus demonstrates that the medium-mediated interaction enhances entanglement generation at the optimum distance from a metal surface.

Superconducting Surface

In the low-frequency regime, the dielectric function of a London superconductor reads

$$\epsilon_s(\omega) = 1 - \frac{c^2}{\omega^2 \lambda_L^2(T)} + i \frac{2c^2}{\omega^2 \delta^2(T)} \quad (26)$$

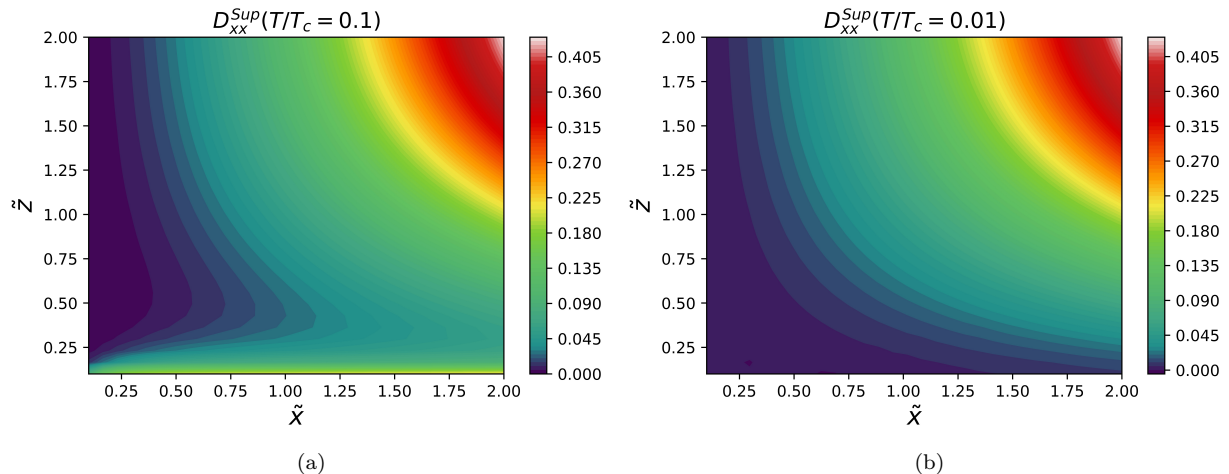


FIG. 5. The contour plot of the relative decay as a function of \tilde{x} , and \tilde{z} near a Niobium superconducting surface at temperature (a) $T/T_c = 0.1 = 0.83$ K and (b) $T/T_c = 0.01 \approx 83$ mK.

Here, the London penetration length and the skin depth are defined as $\lambda_L^2(T) = \lambda_L^2(0)/[1 - (T/T_c)^4]$, and $\delta_L^2(T) = 2/(\omega\mu_0\sigma(T/T_c)^4)$, where $\sigma = 2 \times 10^9 \Omega^{-1}$ represents the electrical conductivity. We consider a superconducting Niobium with $T_c = 8.31$ K and $\lambda_L(0) = 35$ nm at a finite temperature $T = 83.1$ mK. Replacing Eq.(26) into (23), the Fresnel coefficients for a superconducting medium in non-retarded regime are given by

$$r_s \approx 0$$

$$r_p \approx \frac{\delta_L^2(T) - 2i\lambda_L^2(T)}{\delta_L^2(T) - 2i\lambda_L^2(T) - 2\omega^2\delta_L^2(T)\lambda_L^2(T)/c^2} \quad (27)$$

In a non-retarded regime, $D_{xx}^{Sup} \propto \text{Im}[r_p] \propto (T/T_c)^4$ and as a consequence

$$\lim_{(T/T_c) \rightarrow 0} D_{xx}^{Sup} \approx 0 \quad (28)$$

The contour plot of the relative decay is shown in Fig. 5 considering the Niobium superconducting surface at temperature (a) $T = 0.1 T_c$, and (b) $T = 0.01 T_c$. It displays that the relative decay near a superconducting surface behaves the same as near the perfect conductor in a low-temperature regime ($T \ll T_c$), while it tends to behave like a system near the metal surface as the temperature increases to $T \approx T_c$.